ACS APPLIED MATERIALS & INTERFACES

Research Article

www.acsami.org

Enhanced In Vivo Antitumor Efficacy of Doxorubicin Encapsulated within Laponite Nanodisks

Kai Li,[†] Shige Wang,[‡] Shihui Wen,[§] Yueqin Tang,[∥] Jipeng Li,[†] Xiangyang Shi,*[,‡,§] and Qinghua Zhao*[,†]

[†]Department of Orthopaedics, Shanghai First People's Hospital, School of Medicine, Shanghai Jiao Tong University, Shanghai 200080, China

[‡]State Key Laboratory for Modification of Chemical Fibers and Polymer Materials, Donghua University, Shanghai 201620, China

[§]College of Chemistry, Chemical Engineering and Biotechnology, Donghua University, Shanghai 201620, China

[∥]Experiment Center, Shanghai First People's Hospital, School of Medicine, Shanghai Jiao Tong University, Shanghai 200080, China

Supporting Information

ABSTRACT: Development of various nanoscale drug carriers for enhanced antitumor therapy still remains a great challenge. In this study, laponite (LAP) nanodisks encapsulated with anticancer drug doxorubicin (DOX) at an exceptionally high loading efficiency (98.3 ± 0.77%) were used for tumor therapy applications. The long-term in vivo antitumor efficacy and toxicology of the prepared LAP/DOX complexes were analyzed using a tumor-bearing mouse model. Long-term tumor appearance, normalized tumor volume, CD31 staining, and hematoxylin and eosin (H&E)-stained tumor sections were used to evaluate the tumor therapy efficacy, while long-term animal body weight changes and H&E-stained tissue sections of different major organs were used to evaluate the toxicology of LAP/DOX complexes. Finally, the in vivo biodistribution of magnesium ions and DOX in different organs was analyzed. We showed that under the same DOX concentration, LAP/DOX complexes displayed enhanced tumor inhibition efficacy and afforded the treated mice with dramatically prolonged survival time. In vivo biodistribution data revealed that the reticuloendothelial systems (especially liver) had significantly higher magnesium uptake than other major organs, and the LAP carrier was able to be cleared out of the body at 45 days post treatment. Furthermore, LAP/DOX afforded a higher DOX uptake in the tumor region than free DOX, presumably due to the known enhanced permeability and retention effect. The developed LAP-based drug delivery system with an exceptionally high DOX payload, enhanced in vivo antitumor efficacy, and low systemic toxicity may be used as a promising platform for enhanced tumor therapy.

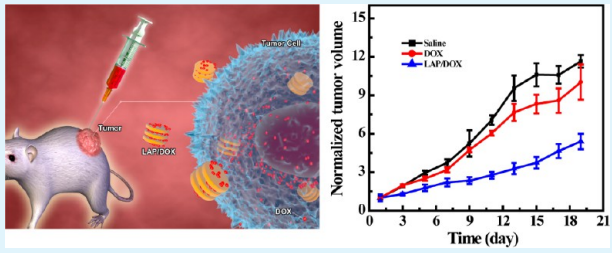

KEYWORDS: *laponite, doxorubicin, antitumor efficacy, systemic toxicity*

INTRODUCTION

Recent advances in nanotechnology have enabled early detection, real-time monitoring and minimally toxic targeted therapy of cancer.[1−3] Despite this progress, cancer is still one of the most challenging diseases to treat and a major cause of mortality and morbidity around the world.[4−7] Conventional chemotherapy is commonly used to prevent cancer cells from multiplying and spreading throughout the body,[2] but it suffers from nonspecific distribution, causing damages to healthy tissue during the treatment.[8] A number of chemotherapeutic drugs, such as doxorubicin (DOX), have a strong tendency to bind with cellular macromolecules, leading to low therapeutic indices.[9] Thus, large doses or repeated administration are usually required to achieve the desired therapeutic effect, which can simultaneously cause a series of severe side effects.[10] Considering the drawbacks of conventional chemotherapy, it is essential to develop various nanoscale delivery systems (e.g., nanoparticles, nanodisks, or nanotubes) for efficient delivery of chemotherapeutic drugs to cancer cells.[8,11−17]

The advantages of nanoscale drug delivery system include passive targeting to tumor tissue via the enhanced permeability and retention (EPR) effect,[18] easy surface functionalization with biological ligands for active tumor targeting,[19,20] and stimuli-responsive drug release.[21,22] Various nanoparticles, nanodisks, or nanotubes have been used as promising candidates for cancer therapy applications. In particular, as a nanodisk-shaped layered synthetic aluminosilicate clay material, laponite (LAP) has been used as a drug carrier,[23−25] mainly due to the fact that the interlayer spacing of LAP can be used for drug encapsulation with a high retention capacity. Furthermore, it has been reported that LAP can be degraded into nontoxic products.[26]

In our previous study, we have shown that LAP nanodisks can be used to encapsulate anticancer drug doxorubicin (DOX) with an exceptionally high loading efficiency of 98.3 ± 0.77% via ionic exchange along the (001) plane of LAP and surface physical

Received: April 6, 2014
Accepted: July 7, 2014
Published: July 7, 2014

adsorption. The formed LAP/DOX nanodisks demonstrated a pH-dependent in vitro drug release profile with higher release rate at an acidic pH condition (pH = 5.4) than at physiological pH condition (pH = 7.4). Most strikingly, the LAP/DOX enabled an enhanced cellular internalization of DOX, and thus having significantly improved in vitro therapeutic efficacy.[27] To move forward from the encouraging in vitro results and further explore the application of LAP as a novel drug carrier, it is reasonable to explore the in vivo antitumor activity and toxicology of LAP/DOX complexes.

In this present research, we used a tumor-bearing mouse model to investigate the in vivo antitumor efficacy and toxicology of the prepared LAP/DOX nanodisks. Long-term tumor appearance, normalized tumor volume, and CD31 and hematoxylin and eosin (H&E) staining of tumor sections were used to evaluate the tumor inhibition efficacy, while long-term body weight and H&E-stained tissue sections of different major organs were compared before and after different treatments (i.e., treated with saline, free DOX, or LAP/DOX) to evaluate the LAP/DOX toxicology. Finally, the in vivo biodistribution of magnesium ions and DOX in different organs was analyzed to understand the long-term fate of LAP and the in vivo distribution of DOX. To our knowledge, this is the first report related to the in vivo study of the therapeutic efficacy of LAP/DOX complexes. Given the fact that the interlayer space and outer surface of LAP nanodisks can be used to efficiently encapsulate various drugs and other small molecules, we anticipate that LAP, as a kind of cost-effective, abundantly available, and biocompatible clay material may be used as a versatile carrier system for various biomedical applications.

EXPERIMENTAL SECTION

Materials. LAP and DOX (in a form of hydrochloride, unless otherwise stated, the used term of DOX indicates DOX·HCl) were purchased from Zhejiang Institute of Geologic and Mineral Resources (China) and Beijing Huafeng Pharmaceutical Co., Ltd. (China), respectively. Human epidermoid carcinoma (KB) cells were obtained from the Institute of Biochemistry and Cell Biology (the Chinese Academy of Sciences, Shanghai, China). Roswell Park Memorial Institute-1640 (RPMI-1640), fetal bovine serum (FBS), penicillin, and streptomycin were from Hangzhou Jinuo Biomedical Technology (Hangzhou, China). All other chemicals were obtained from Aldrich and were used as received. The water used in all experiments was purified using a Milli-Q Plus 185 water purification system (Millipore, Bedford, MA) with a resistivity higher than 18 MΩ·cm.

Loading of DOX within LAP Nanodisks. LAP/DOX nanodisks were prepared according to protocols described in our previous work.[27] In brief, 10 mL of LAP aqueous solution at a concentration of 6 mg/mL was mixed with 10 mL of DOX aqueous solution (2 mg/mL) under magnetic stirring for 24 h to allow LAP to thoroughly swell and interact with DOX. LAP/DOX nanodisks with an optimized loading efficiency of 98.3 ± 0.77% were obtained by centrifugation (8,000 rpm, 5 min). The disks were then rinsed with water for 3 times, air-dried, and stored under dark conditions at room temperature before characterization and use. FTIR spectrometry was performed using a Nicolet Nexus 670 FTIR (Nicolet-Thermo) spectrometer. All spectra were recorded using a transmission mode with a wavenumber range of 650−4000 cm^{-1}. TEM was performed using a JEOL 2010F analytical electron microscope operating at 200 kV. A diluted aqueous suspension (5 μL) of each sample was deposited onto a carbon-coated copper grid and air-dried before measurements.

Cell Cultures and Tumor Models. KB cells were continuously cultured in 25 cm^2 tissue culture flasks with 5 mL of RPMI-1640 medium containing 10% FBS, 100 unit/mL penicillin, and 100 μg/mL streptomycin in a humidified incubator with 5% CO_2 at 37 °C. Animal experiments were performed according to protocols approved by the Shanghai Jiongtong University Laboratory Animal Center and were in accordance with the policies of National Ministry of Health. Female Balb/c nude mice (4−6 weeks old) were obtained from Shanghai Slac Laboratory Animal Center (Shanghai, China). A tumor model was generated by subcutaneous injection of 3×10^6 KB cells in 200 μL of serum free RPMI-1640 culture medium into the back of each Balb/c mouse.

In Vivo Tumor Therapy of LAP/DOX Complexes. When the tumor nodules attained a volume of 0.5−1 cm^3 at approximately 2 weeks post treatment, mice were randomly divided into 3 groups (n = 6 for each group): LAP/DOX treatment group, free DOX treatment group, and control group treated with saline. Each mouse was intratumorally injected with 100 μL saline containing LAP/DOX or free DOX at a DOX concentration of 0.74 mg/mL. In the control group, each mouse was injected with 100 μL saline. The relative tumor volume (denoted V/V_0, where V_0 is the tumor volume when the treatment was initiated, i.e., day 0), body weight and tumor appearance of each mouse were recorded at different time points. The survival time of the mice in each group was also monitored. For the systemic DOX distribution analysis, the tumor-bearing mice were randomly divided into two groups (n = 3 for each group at each time point): LAP/DOX group and free DOX group. The mice treated with 100 μL saline containing LAP/DOX or free DOX at a DOX concentration of 0.74 mg/mL were anesthetized on days 7 and 14. Organs including tumor, heart, liver, spleen, lung, and kidney were harvested. A maximum of 0.3 g of each organ was weighted and grinded with 500 μL lysis solution using a tissue grinder. Then, 200 μL of the resulted solution was mixed with 100 μL of triton and homogenized in 1 mL extraction solution (0.75 mM HCl in isopropanol), and incubated at 37 °C overnight. The supernatant obtained after centrifugation at 12000 rpm for 10 min was analyzed using a multifunctional ELIASA reader (Biotek, Synergy 2) to record the DOX fluorescence (λ_{ex}= 485 nm, λ_{em} = 528 nm). The DOX content was calculated from a standard calibration curve. The relative DOX percentage (%) was calculated by dividing the DOX amount in a specific organ/tumor by the sum of DOX amount in all the specified organs (including heart, liver, spleen, lung, and kidney) and tumor.

To understand the long-term in vivo fate of LAP, tumor-bearing Balb/c nude mice were used. Four mice intratumorally injected with LAP/DOX ([DOX] = 0.74 mg/mL, in 100 μL saline) were euthanized at 1, 3, 14, and 21 days post treatment (one mouse for each time point), respectively. Then, major organs, including the heart, liver, spleen, lung, and kidney were collected and weighed. The organs were digested by aqua regia solution overnight. The magnesium uptake in different organs was then quantified by a Leeman Prodigy inductively coupled plasma-optical emission spectroscopy (ICP-OES, Hudson, NH).

Blood Examination. Healthy Kunming mice (4−6 weeks old, Shanghai Slac Laboratory Animal Center) were randomly divided into 4 groups (n = 2 for each group, one mouse for each time point), and intravenously injected with 100 μL saline (control group), or 100 μL saline containing LAP/DOX ([DOX] = 0.74 mg/mL), free DOX ([DOX] = 0.74 mg/mL), or LAP (2.2 mg/mL, similar to the concentration of LAP used to encapsulate 0.74 mg/mL DOX deduced from the DOX loading percentage of 32.8 ± 2.6%),[27] respectively. On the day 7 and day 14 post treatment, each mouse was anesthetized and the heart was punctured to collect blood. Routine blood test including white blood cell (WBC), hemoglobin (Hb), and platelet (PLT) were recorded on Sysmex XS-800i automated hematology analyzer. Then, blood was centrifuged and supernatant was used to test the serum biochemistry parameters such as aspartate aminotransferase (AST), alanine aminotransferase (ALT), total bilirubin, creatinine, and carbamide using Beckman Coulter Unicel DxC 800 automatic biochemical analyzer.

Histology Examinations. Histological analyses were performed to evaluate the antitumor efficacy and in vivo biosafety of LAP/DOX complexes. To evaluate the antitumor efficacy, 3 tumor-bearing mice were intratumorally injected with saline (100 μL), LAP/DOX ([DOX] = 0.74 mg/mL, in 100 μL saline), and free DOX ([DOX] = 0.74 mg/mL, in 100 μL saline), respectively. Each mouse was euthanized on day 19 post treatment, and the tumor was harvested for H&E staining. To assess the antitumor efficacy of LAP/DOX complexes, 8 tumor-bearing

Scheme 1. Schematic Illustration of the Encapsulation of DOX into LAP Nanodisks (a) and the Cellular Uptake of the LAP/DOX Complexes for in Vitro and in Vivo Antitumor Therapy (b)

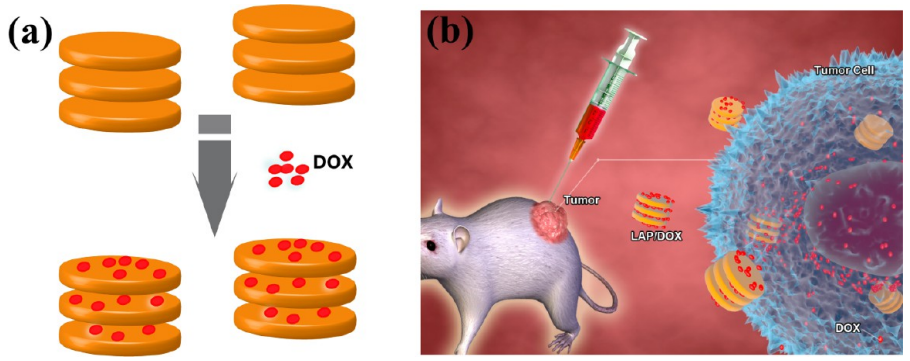

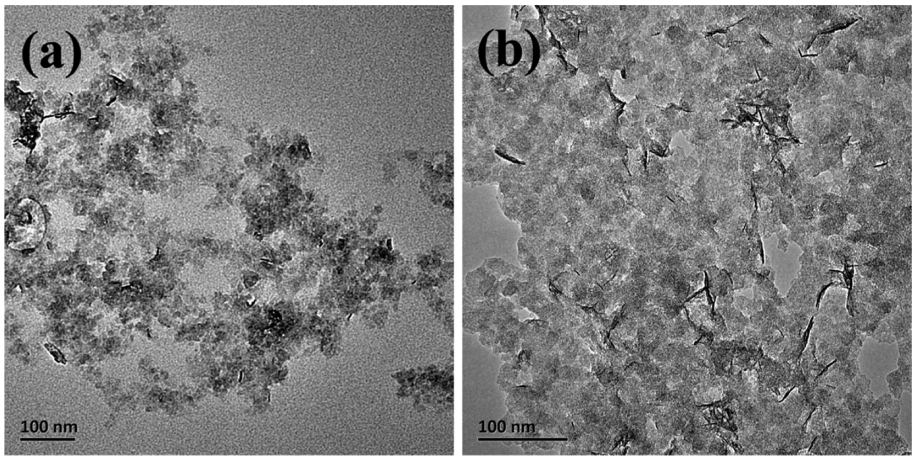

Figure 1. TEM images of (a) LAP and (b) LAP/DOX nanodisks.

mice were randomly divided into 4 groups (n =2 for each group, one mouse for each time point). The mice were intratumorally injected with 100 μL saline (control group), or 100 μL saline containing LAP (2.2 mg/mL), free DOX ([DOX] = 0.74 mg/mL), and LAP/DOX complexes ([DOX] = 0.74 mg/mL), respectively. Mice were euthanized after 7 or 14 days of treatment and different tumor sections were stained using an antibody against endothelial marker, CD31 (BD Pharmingen, San Diego, CA) according to the manufacturer's instruction.

To evaluate the in vivo biosafety, two healthy Kunming mice intravenously injected with saline (100 μL) and LAP/DOX complexes ([DOX] = 0.74 mg/mL, in 100 μL saline), respectively were euthanized after 45 days, and the major organs, including the heart, liver, spleen, lung, and kidney were harvested. The organs were fixed with 10% neutral buffered formalin, embedded in paraffin, sectioned into slices with thickness of 8 μm, stained with H&E, and examined using a Leica DM IL LED inverted phase contrast microscope.

Statistical Analysis. One way ANOVA statistical analysis was performed to evaluate the significance of the experimental data. 0.05 was selected as the significance level, and the data were indicated with (*) for $p < 0.05$, (**) for $p < 0.01$, and (***) for $p < 0.001$, respectively.

RESULTS AND DISCUSSION

Formation and Characterization of LAP/DOX Complexes. LAP nanodisks possess a unique 2-dimensional layered structure with 6 octahedral magnesium ions between 2 layers of 4 tetrahedral silicon atoms.[28] The unique structural characteristics of LAP make it possible to efficiently encapsulate drug molecules within the LAP interlayer space.[23,24,29] In our previous study, we have successfully loaded DOX within LAP nanodisks at an exceptionally high loading efficiency of 98.3 ± 0.77%.[27] It should be noted that the mentioned value of 98.3% is only associated with the DOX loading efficiency, and not associated with the DOX loading percentage (or loading capacity). The mechanistic study of DOX loading within LAP nanodisks has been performed in our previous study.[27] Our results from XRD and zeta-potential measurements have shown that DOX are able to be loaded inside the interlayer space of LAP via ionic exchange, and onto the surface of LAP via electrostatic interaction or hydrogen bonding interaction (Scheme 1a). Since the zeta potential of LAP nanodisks changed from −37.9 ± 1.31 to −10.8 ± 0.53 mV after DOX loading, it is not likely to draw a conclusion that the amount of 1 mg of DOX per 3 mg of LAP would require a complete coverage of the clay and more. In this present study, the formed LAP/DOX nanodisks were used to treat a xenografted tumor model for in vivo tumor therapy applications.

The morphology of LAP nanodisks before and after DOX loading was first investigated using TEM (Figure 1). Obviously, the pristine LAP nanodisks display a regular disk shape with a diameter of 21 ± 3.1 nm. After DOX loading, the disk-like shape was not altered, and the diameter of LAP/DOX was estimated to be 22 ± 2.7 nm, implying that the loading process does not significantly alter the LAP morphology. It is worth noting that the somewhat aggregated LAP nanodisks shown in the TEM images may be caused by the air-drying of the aqueous suspension of the samples during TEM sample preparation, in agreement with previous literature.[30,31] The loading of DOX within LAP nanodisks was qualitatively confirmed using FTIR spectroscopy (Figure S1, Supporting Information). Detailed assignment of various bands of LAP and LAP/DOX sample can be found in our previous study.[27] Similar to our previous study, some distinctive

bands at 1712, 1582, 1412, and 1285 cm^{-1} belonging to DOX are present in the spectrum of LAP/DOX nanodisks, implying the successful encapsulation of DOX within the LAP nanodisks.

In Vivo Antitumor Efficacy of LAP/DOX Complexes. To evaluate the in vivo antitumor efficacy of LAP/DOX complexes, a xenografted KB tumor model was established. A representative photo of KB tumor-bearing mice before treatment can be seen in Figure S2a (Supporting Information). Clearly, after subcutaneously injecting 3×10^6 KB cells on the mouse back, a lump with an approximate volume of 0.55 cm^3 appeared on the back of nude Balb/c mice. Further H&E staining results (Figure S2b, Supporting Information) showed the appearance of tumor cells, confirming the successful construction of KB xenografted tumor model.

The *in vivo* antitumor efficacy of LAP/DOX complexes was then investigated upon intratumoral injection. As shown in Figure 2, the tumor growth rate of mice injected with LAP/DOX complexes was much slower than that of mice treated with free DOX or saline. The appearance of the subcutaneous tumor before treatment and at 19 days post treatment was also recorded using vernier calipers (Figure S3, Supporting Information). It is clear that before treatment (day 0), the tumor size was essentially the same (approximately 0.55 cm^3) for the three different groups. After 19 days, the tumors of the mice treated with free DOX or saline have a volume of 3.69 cm^3 and 5.48 cm^3, respectively and the surrounding multiple irregular blood vessels, especially for mice treated with saline can be observed. In contrast, the tumors treated with LAP/DOX complexes showed much slower growth (3.22 cm^3) and less visible surface blood vessels can be seen when compared to the free DOX and saline groups. The tumor volume follows the order of saline > free DOX > LAP/DOX complexes.

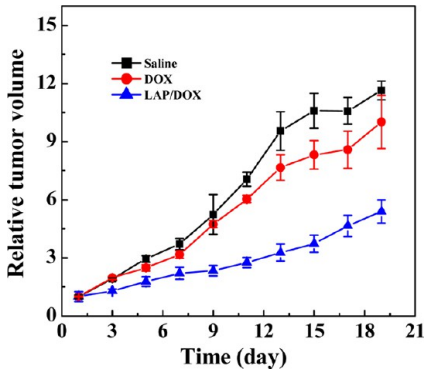

Figure 2. Growth of KB xenografted tumors after various treatments. The relative tumor volumes were normalized according to their initial sizes (mean ± SD, $n = 6$).

Our results indicate the enhanced antitumor efficacy of LAP/DOX complexes.

The tumor inhibition efficacy was confirmed via H&E staining of tumor sections (Figure 3). For saline-treated tumor (Figure 3a), well-defined tumor tissues stained in blue can be clearly seen throughout the whole slice. A large portion of tumor tissue (stained in blue) and a small portion of normal tissue (stained in pink) can be seen in the free DOX-treated tumor (Figure 3b), demonstrating the inhibition efficacy of free DOX. As opposed to saline and free DOX group, in the tumor section treated by LAP/DOX complexes (Figure 3c), a majority of normal tissue stained in pink and only a small portion of tumor tissue stained in blue can be seen. The clear histological differences further demonstrate the enhanced therapeutic efficacy of LAP/DOX complexes.

The antitumor efficacy of LAP/DOX complexes was further assessed by in vivo immunohistochemistry toward the endothelial cancer marker (CD31) expression using an avidin–biotin complex protocol on paraffin-embedded tissue. CD31-positive tumor microvessels were stained to have a brown color, and the lower expression of CD31 implies the higher suppression of angiogenesis, thus a stronger inhibition of cancer cells.[14,32] As shown in Figure 4, on day 7 and day 14, in comparison to tumor mice treated with saline and LAP without DOX complexation, mice-treated with DOX and LAP/DOX complexes showed an obvious decrease in the expression of CD31-positive tumor microvessels, clearly indicating that DOX and LAP/DOX complexes can effectively damage tumor neovascularization. This is likely due to the known fact that DOX can act on the S-phase of cancer cell cycle and thus cause cell death by damaging DNA and its synthesis.[33] In particular, the microvessel density of tumor treated with LAP/DOX complexes (Figure 4d, day 7, and Figure 4h, day 14) was obviously much lower than that of free DOX group (Figure 4c, day 7, and Figure 4g, day 14), implying that LAP/DOX complexes have a better tumor inhibition efficacy than free DOX. As shown in Scheme 1b, the enhanced tumor inhibition efficacy is presumably due to the fact that the encapsulation of DOX within LAP nanodisks enables enhanced cellular uptake of DOX.[27] Likewise, the intratumorally injected LAP/DOX complexes were able to release DOX with a faster rate under the acidic tumor microenvironment than under physiological environment and therefore significantly inhibiting tumor growth. On the other hand, the passive tumor targeting and accumulation of the LAP/DOX nanodisks via the known EPR effect may afford enhanced tumor uptake of DOX to exert enhanced therapeutic efficacy. In contrast, the intratumorally injected free DOX that diffused into cancer cells may be easily pumped out of the cancer cells by the P-glycoprotein and/or other proteins sensitive to free DOX molecules located in the plasma, thus compromising its antitumor efficacy.[34]

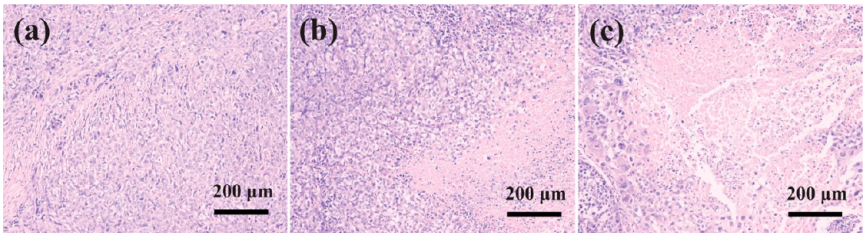

Figure 3. Representative H&E staining images of KB xenografted tumors treated with (a) saline, (b) free DOX, and (c) LAP/DOX complexes on day 19, respectively.

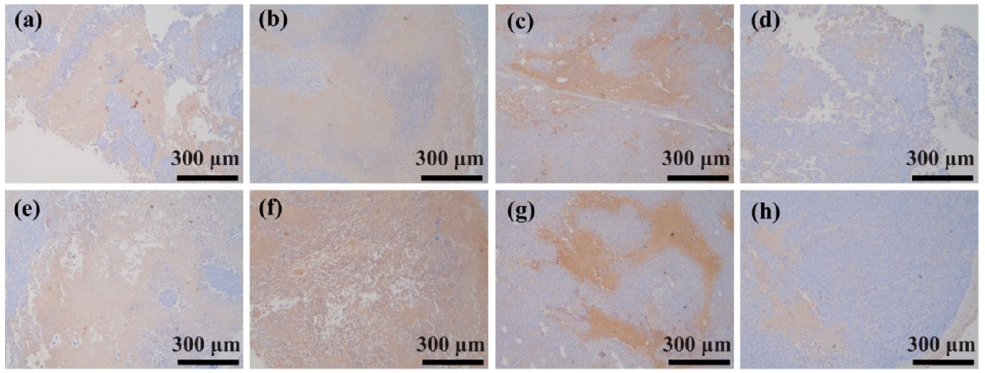

Figure 4. Immunohistochemical staining for CD31 expression of tumor sections in mice after 7 (a–d) and 14 days (e–h) treatment with saline (a and e), LAP (b and f), free DOX (c and g), and LAP/DOX complexes (d and h).

The enhanced tumor uptake of DOX after injection of LAP/DOX complexes was confirmed by in vivo biodistribution analysis of DOX in tumors and in various organs (Figure 5). For

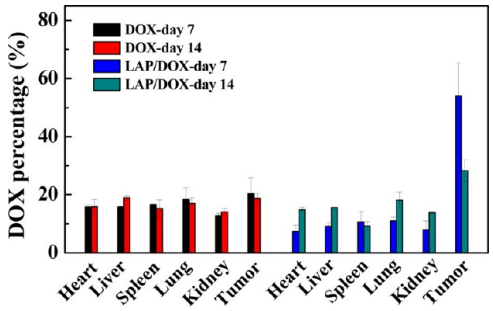

Figure 5. In vivo biodistribution of DOX after 7 and 14 days treatment with free DOX and LAP/DOX complexes (mean ± SD, n = 3).

mice treated with free DOX, DOX was almost distributed equally in tumors and in other organs on day 7 and day 14. The amount of DOX showed no obvious change with time extending. For LAP/DOX complexes, about 50% of the total DOX uptaken by the tumor and the specified main organs was found in the tumor tissue on day 7. This percentage decreased to 28.3 ± 3.7% on day 14. The LAP/DOX complexes afforded a higher DOX uptake in the tumor tissue than free DOX (54.0 ± 11.3% versus 24.5 ± 5.4% on day 7, and 28.3 ± 3.7% versus 18.7 ± 1.6% on day 14, respectively). Our data suggest that the nanoscale LAP/DOX complexes are able to be accumulated in the tumor region via a passive EPR effect,[18] thereby exerting more significant tumor inhibition effect than free DOX.

The survival time of the mice in each group was also monitored, and the long-term survival rate was calculated by dividing the number of surviving mice by the number of total mice at the beginning of treatment to further illustrate the antitumor therapeutic effect (Figure 6). For the saline group, abnormal proliferation and metastasis led to one mouse death on day 32. With the time post treatment, uncontrollable mouse death occurred on day 35 (2 mice died) and day 41 (1 mouse died), and on day 47 all the remaining mice died. The survival rate of mice treated with free DOX was better to a certain extent with an average life-span of approximately 8 days, partially due to the antitumor effect of free DOX. For the LAP/DOX treated group, the first mouse death occurred on day 42, longer than the mice treated with free DOX (day 34) or saline (day 32). Additionally, 2 of the 6 mice were still alive after 60 days. This

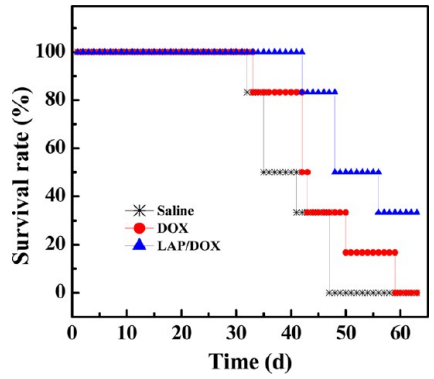

Figure 6. Survival rate of mice as a function of the time post treatments with saline, free DOX, and LAP/DOX complexes.

further confirms the improved antitumor efficacy of LAP/DOX complexes, affording prolonged survival time of the tumor mice.

Systemic Toxicity. For in vivo antitumor therapy applications of LAP/DOX complexes, it is essential to explore the long-term fate of the intratumorally injected LAP carrier. The biodistribution of the LAP was investigated after intratumoral injection of the LAP/DOX complexes. By quantitatively measuring the concentration of magnesium ions in different organs (including the heart, liver, spleen, lung, and kidney) at 1, 3, 14, and 21 days post treatment using ICP-OES, we were able to estimate the distribution of LAP carrier (Figure 7). It is clear that at all time points post treatment, the heart, lung, and kidney have

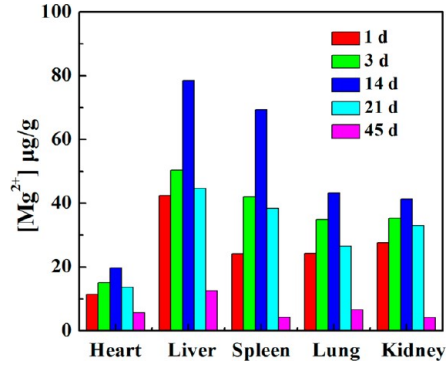

Figure 7. Biodistribution of magnesium element in major organs of the mice, including the heart, liver, spleen, lung, and kidney at different time points post treatment with LAP/DOX complexes (one mouse was used for each time point).

dx.doi.org/10.1021/am502094a | ACS Appl. Mater. Interfaces 2014, 6, 12328–12334

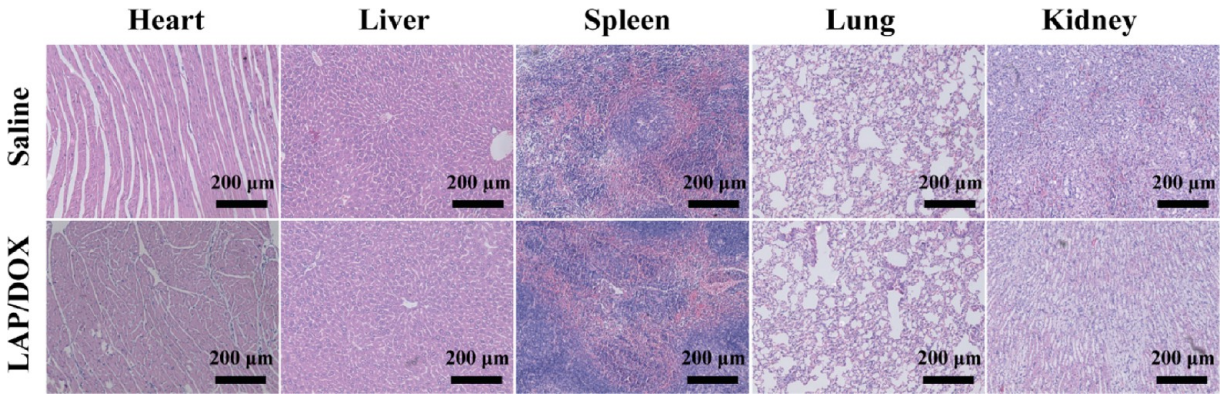

Figure 8. H&E-stained tissue sections of major organs, including the heart, liver, spleen, lung, and kidney from Kunming mice treated with saline or LAP/DOX complexes on day 45.

relatively lower magnesium uptake. In sharp contrast, the reticuloendothelial systems (RES, liver and spleen, especially liver) have significantly higher magnesium uptake of 42.5 (1 d), 50.3 (3 d), 78.5 (14 d), and 44.6 μg/g (21 d) in the liver and 24.1 (1 d), 42.1 (3 d), 69.3 (14 d), and 38.4 μg/g (21 d) in the spleen, respectively. These differences in magnesium uptake indicate that LAP/DOX complexes are able to be translocated from the tumor site to the RES via blood or lymphatic circulation.[35] The magnesium level in all of the studied organs obviously decreased at 14 days post treatment, and at 45 days post treatment, the magnesium levels were too low to be detected, suggesting the nearly complete LAP clearance in the treated mice via the RES and blood or lymphatic circulation.

Finally, the *in vivo* biosafety of LAP/DOX complexes was investigated to further illustrate the advantages of LAP as an antitumor drug carrier. In our previous study, we have shown that LAP nanodisks do not display apparent in vitro cytotoxicity in the given concentration range.[27] In this study, we further studied the in vivo compatibility of LAP using serum biochemistry assay and complete blood panel test together with histological examinations. On the day 7 and day 14 post treatment, mice were anesthetized and heart was punctured for blood test. As shown in Table S1 and Table S2 (Supporting Information), at 7 and 14 days post treatment, there was no physiological difference in blood routine parameters (Supporting Information Table S1) including Hb, WBC, and PLT, as well as serum biochemistry parameters (Supporting Information Table S2) including AST, ALT, total bilirubin, creatinine and carbamide among groups treated with saline, LAP, and LAP/DOX complexes. These results clearly indicate that mice treated with saline, LAP and LAP/DOX complexes are still quite healthy. However, compared with mice treated with LAP/DOX complexes, free DOX-treated mice showed decreased blood routine parameters and serum biochemistry parameters (Supporting Information Tables S1 and S2), which is likely associated with the systemic toxicity of DOX. Given the fact that the mice were treated with LAP/DOX and free DOX at similar DOX concentration, we can conclude that LAP/DOX complexes induce much lower systemic toxicity than free DOX.

At 45 days post treatment, mice treated with LAP/DOX complexes were euthanized, and the major organs including the heart, liver, spleen, lung, and kidney, were collected for pathological examination via H&E staining (Figure 8). All of the studied organs from the mouse treated with LAP/DOX showed no appreciable abnormality or noticeable organ damage when compared to the saline group, suggesting a good biocompatibility of LAP/DOX complexes, as well as LAP alone, in mice. The body weight of mice in different groups was also monitored (Figure S4, Supporting Information). Mice treated with LAP/DOX complexes showed no obvious variation in weight over time compared to the mice treated with saline, further indicating that neither LAP/DOX nor LAP is toxic to mice. Therefore, LAP can be safely used in drug delivery systems.

CONCLUSION

In summary, we have investigated the in vivo antitumor efficacy and systemic toxicity of the prepared LAP/DOX nanodisks as a novel anticancer drug delivery system using a tumor-bearing mouse model. Our results reveal that at the same DOX concentration, LAP/DOX complexes are able to inhibit tumor growth more significantly than free DOX, and the survival time of mice treated with LAP/DOX is dramatically longer than the mice treated with free DOX. The enhanced antitumor efficacy of LAP/DOX complexes is believed to be attributed to the nanoscale drug delivery system that can passively target and accumulate in the tumor region via the known EPR effect, which has been demonstrated by the analysis of the in vivo biodistribution of DOX. With the ability to be cleared out of body at 45 days post treatment and proven biocompatibility via histological examinations, the LAP-based drug delivery system with an exceptionally high DOX payload may be used as a promising platform for tumor therapy applications.

ASSOCIATED CONTENT

Supporting Information

Additional materials characterization and in vivo assay data. This material is available free of charge via the Internet at http://pubs.acs.org/.

AUTHOR INFORMATION

Corresponding Authors

*E-mail: xshi@dhu.edu.cn.
*E-mail: sawboneszhao@163.com.

Author Contributions

K.L. and S.W. contributed equally to this work.

Notes

The authors declare no competing financial interest.

ACKNOWLEDGMENTS

This research was supported by grants from the Research Fund for the Doctoral Program of Higher Education of China

(20100073120090, 20130075110004). X.S. thanks the Program for Professor of Special Appointment (Eastern Scholar) at Shanghai Institutions of Higher Learning.

REFERENCES

(1) Kim, K.; Kim, J. H.; Park, H.; Kim, Y.-S.; Park, K.; Nam, H.; Lee, S.; Park, J. H.; Park, R.-W.; Kim, I.-S. Tumor-Homing Multifunctional Nanoparticles for Cancer Theragnosis: Simultaneous Diagnosis, Drug Delivery, and Therapeutic Monitoring. *J. Controlled Release* **2010**, *146*, 219−227.

(2) Shen, J.; He, Q.; Gao, Y.; Shi, J.; Li, Y. Mesoporous Silica Nanoparticles Loading Doxorubicin Reverse Multidrug Resistance: Performance and Mechanism. *Nanoscale* **2011**, *3*, 4314−4322.

(3) Sumer, B.; Gao, J. Theranostic Nanomedicine for Cancer. *Nanomedicine* **2008**, *3*, 137−140.

(4) Jemal, A.; Bray, F.; Center, M. M.; Ferlay, J.; Ward, E.; Forman, D. Global Cancer Statistics. *Ca—Cancer J. Clin.* **2011**, *61*, 69−90.

(5) Jemal, A.; Siegel, R.; Xu, J.; Ward, E. Cancer Statistics, 2010. *Ca—Cancer J. Clin.* **2010**, *60*, 277−300.

(6) Siegel, R.; Naishadham, D.; Jemal, A. Cancer Statistics, 2012. *Ca—Cancer J. Clin.* **2012**, *62*, 10−29.

(7) Siegel, R.; Naishadham, D.; Jemal, A. Cancer Statistics, 2013. *Ca—Cancer J. Clin.* **2013**, *63*, 11−30.

(8) Wen, S.; Liu, H.; Cai, H.; Shen, M.; Shi, X. Targeted and pH-Responsive Delivery of Doxorubicin to Cancer Cells Using Multifunctional Dendrimer-Modified Multi-Walled Carbon Nanotubes. *Adv. Healthcare Mater.* **2013**, *2*, 1267−1276.

(9) Minchinton, A. I.; Tannock, I. F. Drug Penetration in Solid Tumours. *Nat. Rev. Cancer* **2006**, *6*, 583−592.

(10) Kunieda, K.; Seki, T.; Nakatani, S.; Wakabayashi, M.; Shiro, T.; Inoue, K.; Sougawa, M.; Kimura, R.; Harada, K. Implantation Treatment Method of Slow Release Anticancer Doxorubicin Containing Hydroxyapatite (DOX-HAP) Complex. A Basic Study of a New Treatment for Hepatic Cancer. *Br. J. Cancer* **1993**, *67*, 668−673.

(11) Bikram, M.; Gobin, A. M.; Whitmire, R. E.; West, J. L. Temperature-Sensitive Hydrogels with SiO_2-Au Nanoshells for Controlled Drug Delivery. *J. Controlled Release* **2007**, *123*, 219−227.

(12) Kirchner, C.; Liedl, T.; Kudera, S.; Pellegrino, T.; Javier, A. M.; Gaub, H. E.; Stölzle, S.; Fertig, N.; Parak, W. J. Cytotoxicity of Colloidal CdSe and CdSe/ZnS Nanoparticles. *Nano Lett.* **2005**, *5*, 331−338.

(13) Liu, X.; Tao, H.; Yang, K.; Zhang, S.; Lee, S. T.; Liu, Z. Optimization of Surface Chemistry on Single-Walled Carbon Nanotubes for In Vivo Photothermal Ablation of Tumors. *Biomaterials* **2011**, *32*, 144−151.

(14) Wang, Y.; Guo, R.; Cao, X.; Shen, M.; Shi, X. Encapsulation of 2-Methoxyestradiol within Multifunctional Poly(Amidoamine) Dendrimers for Targeted Cancer Therapy. *Biomaterials* **2011**, *32*, 3322−3329.

(15) Yang, K.; Zhang, S.; Zhang, G.; Sun, X.; Lee, S. T.; Liu, Z. Graphene in Mice: Ultrahigh In Vivo Tumor Uptake and Efficient Photothermal Therapy. *Nano Lett.* **2010**, *10*, 3318−3323.

(16) Yavuz, M. S.; Cheng, Y.; Chen, J.; Cobley, C. M.; Zhang, Q.; Rycenga, M.; Xie, J.; Kim, C.; Song, K. H.; Schwartz, A. G. Gold Nanocages Covered by Smart Polymers for Controlled Release with Near-Infrared Light. *Nat. Mater.* **2009**, *8*, 935−939.

(17) Zhang, M.; Guo, R.; Wang, Y.; Cao, X.; Shen, M.; Shi, X. Multifunctional Dendrimer/Combretastatin A4 Inclusion Complexes Enable In Vitro Targeted Cancer Therapy. *Int. J. Nanomed.* **2011**, *6*, 2337−2349.

(18) Liu, Z.; Chen, K.; Davis, C.; Sherlock, S.; Cao, Q.; Chen, X.; Dai, H. Drug Delivery with Carbon Nanotubes for In Vivo Cancer Treatment. *Cancer Res.* **2008**, *68*, 6652−6660.

(19) Brannon-Peppas, L.; Blanchette, J. O. Nanoparticle and Targeted Systems for Cancer Therapy. *Adv. Drug Delivery Rev.* **2012**, *64*, 206−212.

(20) Chen, Q.; Li, K.; Wen, S.; Liu, H.; Peng, C.; Cai, H.; Shen, M.; Zhang, G.; Shi, X. Targeted CT/MR Dual Mode Imaging of Tumors Using Multifunctional Dendrimer-Entrapped Gold Nanoparticles. *Biomaterials* **2013**, *34*, 5200−5209.

(21) Li, D.; Tang, J.; Guo, J.; Wang, S.; Chaudhary, D.; Wang, C. Hollow-Core Magnetic Colloidal Nanocrystal Clusters with Ligand-Exchanged Surface Modification as Delivery Vehicles for Targeted and Stimuli-Responsive Drug Release. *Chem.—Eur. J.* **2012**, *18*, 16517−16524.

(22) Pan, Y.-J.; Chen, Y.-Y.; Wang, D.-R.; Wei, C.; Guo, J.; Lu, D.-R.; Chu, C.-C.; Wang, C.-C. Redox/pH Dual Stimuli-Responsive Biodegradable Nanohydrogels with Varying Responses to Dithiothreitol and Glutathione for Controlled Drug Release. *Biomaterials* **2012**, *33*, 6570−6579.

(23) Jung, H.; Kim, H. M.; Choy, Y. B.; Hwang, S. J.; Choy, J. H. Itraconazole-Laponite: Kinetics and Mechanism of Drug Release. *Appl. Clay Sci.* **2008**, *40*, 99−107.

(24) Jung, H.; Kim, H. M.; Choy, Y. B.; Hwang, S. J.; Choy, J. H. Laponite-Based Nanohybrid for Enhanced Solubility and Controlled Release of Itraconazole. *Int. J. Pharm.* **2008**, *349*, 283−290.

(25) Viseras, C.; Cerezo, P.; Sanchez, R.; Salcedo, I.; Aguzzi, C. Current Challenges in Clay Minerals for Drug Delivery. *Appl. Clay Sci.* **2010**, *48*, 291−295.

(26) Li, Y.; Maciel, D.; Tomás, H.; Rodrigues, J.; Ma, H.; Shi, X. pH Sensitive Laponite/Alginate Hybrid Hydrogels: Swelling Behaviour and Release Mechanism. *Soft Matter* **2011**, *7*, 6231−6238.

(27) Wang, S.; Wu, Y.; Guo, R.; Huang, Y.; Wen, S.; Shen, M.; Wang, J.; Shi, X. Laponite Nanodisks as an Efficient Platform for Doxorubicin Delivery to Cancer Cells. *Langmuir* **2013**, *29*, 5030−5036.

(28) Herrera, N. N.; Letoffe, J. M.; Putaux, J. L.; David, L.; Bourgeat-Lami, E. Aqueous Dispersions of Silane-Functionalized Laponite Clay Platelets. A First Step toward the Elaboration of Water-Based Polymer/Clay Nanocomposites. *Langmuir* **2004**, *20*, 1564−1571.

(29) Wang, S.; Zheng, F.; Huang, Y.; Fang, Y.; Shen, M.; Zhu, M.; Shi, X. Encapsulation of Amoxicillin within Laponite-Doped Poly(Lactic-co-glycolic acid) Nanofibers: Preparation, Characterization and Antibacterial Activity. *ACS Appl. Mater. Interfaces* **2012**, *4*, 6393−6401.

(30) Ge, S.; Shi, X. Y.; Sun, K.; Li, C. P.; Uher, C.; Baker, J. R., Jr.; Banaszak Holl, M. M.; Orr, B. G. Facile Hydrothermal Synthesis of Iron Oxide Nanoparticles with Tunable Magnetic Properties. *J. Phys. Chem. C* **2009**, *113*, 13593−13599.

(31) Shi, X. Y.; Wang, S. H.; Swanson, S. D.; Ge, S.; Cao, Z. Y.; Van Antwerp, M. E.; Landmark, K. J.; Baker, J. R., Jr. Dendrimer-Functionalized Shell-Crosslinked Iron Oxide Nanoparticles for In-Vivo Magnetic Resonance Imaging of Tumors. *Adv. Mater.* **2008**, *20*, 1671−1678.

(32) Wang, Y.; Liu, P.; Duan, Y.; Yin, X.; Wang, Q.; Liu, X.; Wang, X.; Zhou, J.; Wang, W.; Qiu, L. Specific Cell Targeting with APRPG Conjugated PEG-PLGA Nanoparticles for Treating Ovarian Cancer. *Biomaterials* **2014**, *35*, 983−992.

(33) Zheng, F.; Wang, S.; Shen, M.; Zhu, M.; Shi, X. Antitumor Efficacy of Doxorubicin-Loaded Electrospun Nano-Hydroxyapatite-Poly-(Lactic-co-glycolic acid) Composite Nanofibers. *Polym. Chem.* **2013**, *4*, 933−941.

(34) Goren, D.; Horowitz, A. T.; Tzemach, D.; Tarshish, M.; Zalipsky, S.; Gabizon, A. Nuclear Delivery of Doxorubicin via Folate-Targeted Liposomes with bypass of Multidrug-Resistance Efflux Pump. *Clin. Cancer Res.* **2000**, *6*, 1949−1957.

(35) Wang, C.; Tao, H.; Cheng, L.; Liu, Z. Near-Infrared Light Induced In Vivo Photodynamic Therapy of Cancer Based on Upconversion Nanoparticles. *Biomaterials* **2011**, *32*, 6145−6154.